



Ultrafast Fourier Transform with a Femtosecond-Laser-Driven Molecule

Kouichi Hosaka,^{1,2} Hiroyuki Shimada,^{1,2} Hisashi Chiba,^{1,2} Hiroyuki Katsuki,^{1,2,3} Yoshiaki Teranishi,^{2,4}
Yukiyoshi Ohtsuki,^{2,4} and Kenji Ohmori^{1,2,3,*}

¹*Institute for Molecular Science, National Institutes of Natural Sciences, Myodaiji, Okazaki 444-8585, Japan*

²*CREST, Japan Science and Technology Agency, Kawaguchi, Saitama 332-0012, Japan*

³*The Graduate University for Advanced Studies (SOKENDAI), Shonan Village, Hayama, Kanagawa 240-0193, Japan*

⁴*Department of Chemistry, Graduate School of Science, Tohoku University, Sendai 980-8578, Japan*

(Received 7 January 2010; published 3 May 2010)

Wave functions of electrically neutral systems can be used as information carriers to replace real charges in the present Si-based circuit, whose further integration will result in a possible disaster where current leakage is unavoidable with insulators thinned to atomic levels. We have experimentally demonstrated a new logic gate based on the temporal evolution of a wave function. An optically tailored vibrational wave packet in the iodine molecule implements four- and eight-element discrete Fourier transform with arbitrary real and imaginary inputs. The evolution time is 145 fs, which is shorter than the typical clock period of the current fastest Si-based computers by 3 orders of magnitudes.

DOI: 10.1103/PhysRevLett.104.180501

PACS numbers: 03.67.Lx, 33.80.-b, 42.50.Dv, 82.53.Kp

The present Si-based circuit will shortly reach its fundamental limit where the current leakage will cause heat and errors with insulators thinned to atomic levels [1]. This limit cannot be overcome even with sophisticated molecular electronics [2] as long as real charges are used as information carriers. Wave functions of electrically neutral systems can possibly replace real charges of the present Si-based circuits to avoid this leakage problem. Neutral atoms and molecules are good candidates as these neutral systems. Furthermore, a shaped ultrashort laser pulse can access many eigenstates simultaneously in an atom or molecule. It is not unrealistic that 10 vibrational eigenstates in a diatomic molecule are coherently superposed to generate a vibrational wave packet (WP):

$$|\Psi(r, t)\rangle = \sum_n c_n |\psi_n(r)\rangle \exp[-i(\omega_n t - \phi_n)], \quad (1)$$

where $|\psi_n(r)\rangle$ and ω_n are the eigenfunction and transition frequency of the n th vibrational level, respectively; c_n and ϕ_n represent its amplitude and phase; and r is an internuclear distance. The amplitude c_n and phase ϕ_n of each eigenstate can be manipulated individually with a pulse shaper, binarized as (0, 1) and (0, π), for example, to give possible binary codes (0, 0), (0, π), (1, 0), and (1, π). Accordingly $(2^2)^{10} = 1\,048\,576$ different kinds of information can be encoded to the WP in a simple diatomic molecule in the angstrom scale. This inherent property as a high-density memory makes it meaningful to investigate information processing with eigenstates of atoms and molecules. Molecules are especially now expected to be a promising medium for large-scale quantum computing [3–5]; the dipole-dipole interaction of molecules is expected to serve as a useful resource for two-qubit operation based on quantum correlation. Hence it is promising to study information processing with molecular eigenstates, which will be referred to as “molecular eigenstate-based

information processing (MEIP)” hereafter, for both high-density classical information processing and quantum information processing.

Read and write operations are the most fundamental operations in any type of information processing. For MEIP, the read procedure is the retrieval of amplitude and phase information stored in a WP, and the write procedure is the creation of arbitrarily shaped WPs with shaped ultrashort laser pulses. The development of these most fundamental operations is almost finished [6–12].

The next step should be the development of logic gates. A number of theoretical efforts [13–18] and a few experimental efforts [19,20] have been made on logic gates to be implemented in the vibrational, rovibrational, and vibronic manifolds of diatomic and polyatomic molecules, mostly based on population transfer with shaped ultrashort laser pulses. Here we demonstrate new logic gates based on the temporal evolution of a vibrational WP in a diatomic molecule. We use a WP composed of vibrational levels around $v = 36$ in the B state of the iodine molecule, so the relative phase oscillates at 1.7×10^{12} Hz between the adjacent vibrational levels. This oscillation gives ultrafast phase shift of each eigenfunction to be regarded as the clock rate of this new logic gate. We have applied this free-evolution gate to the discrete Fourier-Transform (DFT), which is one of the most important logic gates and is useful in a variety of sciences and technologies such as spectroscopy and image analysis [21]. It is also a key component in an important quantum algorithm such as Shor’s factorization algorithm [22]. Our ultrahigh-precision wave-packet interferometry [6–8] has retrieved complete sets of amplitude and phase information stored in the input and output states, verifying the transform has been securely executed with arbitrary real and imaginary inputs. The essence of this scheme is summarized in Fig. 1. As for the four-element DFT, for example, an input \mathbf{f}^{in} such as

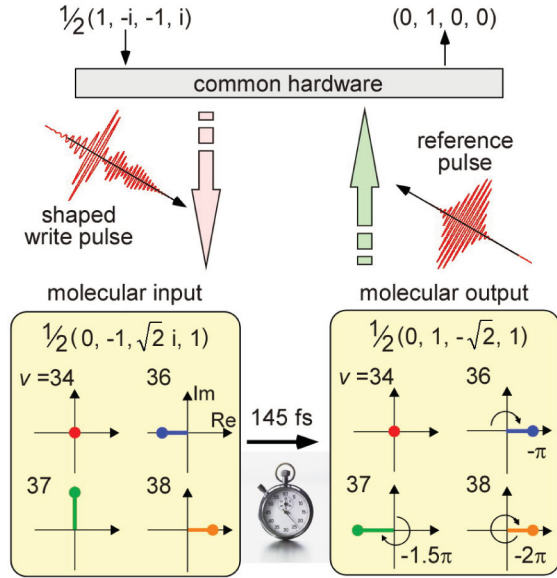


FIG. 1 (color). Schematic of the present DFT with an example: $\frac{1}{2}(1, -i, -1, i) \rightarrow (0, 1, 0, 0)$. The common transform matrices \mathbf{w}_4 and \mathbf{w}_4^{-1} are operated for any arbitrary inputs and outputs, respectively, by the indicated hardware.

$\frac{1}{2}(1, -i, -1, i)$ is base transformed with a matrix \mathbf{w}_4^{-1} to the coefficients vector $\mathbf{a}(t=0) = (a_v(t=0), a_{v+2}(t=0), a_{v+3}(t=0), a_{v+4}(t=0))$ of a set of vibrational eigenstates $v, v+2, v+3$, and $v+4$ in the B state of the iodine molecule:

$$\mathbf{a}(t=0) = \mathbf{w}_4^{-1} \mathbf{f}^{\text{in}}, \quad (2)$$

where the time-dependent coefficients vector $\mathbf{a}(t) = (a_v(t), a_{v+2}(t), a_{v+3}(t), a_{v+4}(t))$ is defined with a time-dependent phase $\delta_v(t)$ as

$$\begin{aligned} a_v(t) |\psi_v(r)\rangle &= c_v e^{i\delta_v(t)} |\psi_v(r)\rangle \\ &= c_v e^{i\delta_v(t=0)} |\psi_v(r)\rangle \exp(-i\omega_v t), \end{aligned} \quad (3)$$

and the 4×4 DFT matrix \mathbf{G}_4 is diagonalized as

$$\mathbf{G}_4 = \mathbf{w}_4 \mathbf{D}_4 \mathbf{w}_4^{-1}. \quad (4)$$

Therefore the DFT \mathbf{f}^{out} of the input \mathbf{f}^{in} is

$$\mathbf{f}^{\text{out}} = \mathbf{G}_4 \mathbf{f}^{\text{in}} = \mathbf{w}_4 \mathbf{D}_4 \mathbf{a}(t=0). \quad (5)$$

Ignoring the potential anharmonicity of the B state, the diagonal matrix \mathbf{D}_4 represents the temporal evolution of $\mathbf{a}(t)$ for $\frac{1}{4}$ of the classical vibrational period T_{vib} :

$$\mathbf{a}(t = \frac{1}{4} T_{\text{vib}}) = \mathbf{D}_4 \mathbf{a}(t=0), \quad (6)$$

where $T_{\text{vib}} = \frac{h}{\Delta E}$, and ΔE is the energy separation of the adjacent vibrational levels. The matrices \mathbf{G}_4 , \mathbf{w}_4 , \mathbf{w}_4^{-1} , and \mathbf{D}_4 are given in the supplementary material [23]. In the actual experiment, therefore, $\mathbf{a}(t=0)$ is written to the vibrational WP with a shaped laser pulse. The coefficients a_v 's of that input WP after its temporal evolution for $\frac{1}{4} T_{\text{vib}}$ are measured to read $\mathbf{a}(t = \frac{1}{4} T_{\text{vib}})$ with our ultrahigh-precision WP interferometry stabilized on the attosecond

time scale. The $\mathbf{a}(t = \frac{1}{4} T_{\text{vib}})$ thus experimentally obtained is finally transformed by \mathbf{w}_4 to give the final output $\mathbf{f}^{\text{out}} = \mathbf{G}_4 \mathbf{f}^{\text{in}}$. It is important to note that the transform matrix \mathbf{w}_4 is common to any arbitrary input \mathbf{f}^{in} and can be physically implemented by a common hardware for both of the transforms \mathbf{w}_4 and \mathbf{w}_4^{-1} . In the classical digital computer, DFT is usually implemented by the fast FT (FFT) algorithm, which reduces the computational steps of the N -element DFT from N^2 to $2N \log_2(N)$ [21]. It is not straightforward to compare our DFT directly with the current FFT algorithm, because we have omitted the base transforms \mathbf{w}_4^{-1} and \mathbf{w}_4 , and the computational steps are reduced to N . However, the residual N -step operation is drastically accelerated with the parallel phase shift of the N functions superposed coherently and with the ultrafast molecular clock. This ultrafast FT (UFFT) is completed in subpicoseconds, which is shorter than the typical clock period of the current fastest Si-based computers by 3 orders of magnitudes [24].

We have tested the performance of our four-element UFFT for four orthogonal inputs, using the vibrational levels $v = 34, 36, 37$, and 38 . Since DFT is a linear transform, the transforms of four basis functions are a sufficient test for arbitrary inputs. To check the basis-set dependence, we have tested with two sets of basis functions shown in Table I. The details of the experimental setup and procedures will be given elsewhere [25], and the relevant molecular inputs and outputs, $\mathbf{a}(t=0)$ and $\mathbf{a}(t = \frac{1}{4} T_{\text{vib}})$, are described in the supplementary material [23]. Briefly, the I_2 molecules were prepared in the electronic ground state ($X^1\Sigma_g^+$) by an expansion of heated I_2 -Ar mixture (~ 330 K, ~ 2 atm) into a vacuum chamber through a nozzle. The output of a Ti: sapphire laser system (pulse width ~ 100 fs, repetition rate 1 kHz) was used to pump an optical parametric amplifier (OPA). Its output was tuned

TABLE I. Orthogonal four-element inputs and their DFTs tested in the present experiments and corresponding preparation fidelities and transform accuracies. Numbers in parentheses indicate 1 standard deviation estimated from 1 standard deviation of the phases of the input and output interferograms least-square fitted with sine functions. The uncertainties in the population spectra were not included in these error limits [23].

\mathbf{f}^{in}	\mathbf{f}^{out}	Preparation fidelity	Transform accuracy
Set 1			
(a)	$(1, 0, 0, 0) \rightarrow \frac{1}{2}(1, 1, 1, 1)$	0.92 (1)	0.97 (2)
(b)	$(0, 1, 0, 0) \rightarrow \frac{1}{2}(1, i, -1, -i)$	0.948 (5)	0.98 (3)
(c)	$(0, 0, 1, 0) \rightarrow \frac{1}{2}(1, -1, 1, -1)$	0.91 (1)	0.95 (2)
(d)	$(0, 0, 0, 1) \rightarrow \frac{1}{2}(1, -i, -1, i)$	0.956 (2)	0.98 (1)
Set 2			
(e)	$\frac{1}{2}(1, 1, 1, 1) \rightarrow (1, 0, 0, 0)$	0.960 (2)	0.98 (1)
(f)	$\frac{1}{2}(1, i, -1, -i) \rightarrow (0, 0, 0, 1)$	0.94 (2)	0.97 (3)
(g)	$\frac{1}{2}(1, -1, 1, -1) \rightarrow (0, 0, 1, 0)$	0.935 (2)	0.95 (2)
(h)	$\frac{1}{2}(1, -i, -1, i) \rightarrow (0, 1, 0, 0)$	0.944 (5)	0.997 (2)

around ~ 524 nm and was input to our newly developed ultrastable interferometer, in which a liquid crystal pulse shaper was inserted in one of the two arms [23]. This interferometer produced a shaped “write” pulse and an unshaped “reference” pulse whose delay was highly stabilized on the attosecond time scale. The write and reference pulses were introduced collinearly into the vacuum chamber to intersect the molecular jet. The write pulse was used to create the shaped WP at $t \sim -1.2 - 1.5$ ps to prepare an arbitrary molecular input $\mathbf{a}(t=0)$, which evolves into a molecular output $\mathbf{a}(t = \frac{1}{4}T_{\text{vib}} \sim 145$ fs) with the present choice of v . The reference pulse was used to create a reference WP at $t = 0$ or ~ 145 fs. We employed a narrow-band nanosecond “read” laser pulse delayed from the write pulse by 35 ns for the state-selective interrogation by the laser-induced fluorescence technique with the E state being the fluorescent state. The wavelength of this read pulse was scanned to measure the E - B excitation spectra of the $v_E \leftarrow v = 27 \leftarrow 34, 29 \leftarrow 36, 28 \leftarrow 37$, and $29 \leftarrow 38$ vibronic bands without introducing the reference pulse. For each input \mathbf{f}^{in} , we measured the spectra of a shaped input WP, whose areas were normalized, respectively, by those of an unshaped one measured with the pulse shaper set to have its maximum transmissions at all the frequency components of the OPA output. All of the measured spectra will be given elsewhere [25]. A set of these four normalized areas is hereafter referred to as a “population spectrum,” and is shown in Fig. 2 (i) as a histogram. The population of each eigenstate is hereafter defined to be the height of each bar in this histogram. The phases $\delta_v(t)$'s of the eigenstates at $t = 0$ or ~ 145 fs were obtained from the interferogram of the shaped and reference WPs. In this interferogram, we plotted the peak areas of the excitation spectra measured with the reference WP superposed on the shaped WP as a function of their relative phase θ scanned for $6.9 - 8.7\pi$ in steps of $-0.43 - -0.54$ radian toward a negative direction by moving a mechanical stage placed in one arm of the interferometer. In each step, the phase θ was feedback stabilized every 11–16 s in the intervals of the measurements of the vibronic bands. This phase stabilization was turned off during the measurement of each vibronic band. The phases $\delta_v(t)$'s thus measured were not exactly the same as those defined by Eq. (3) since the reference pulse was more or less deviated from a FT-limited one. However, this is not an essential problem in the present demonstration since the phase origins can be redefined to be the phases of the eigenstates of the reference WP. The details of the data analyses will be given elsewhere [25].

Figures 2 (a) and (h) show the experimental results obtained with the inputs listed in Table I (a) and (h). For example, Figure 2 (a) shows the result with the input $\mathbf{f}^{\text{in}} = (1, 0, 0, 0)$ transformed to the molecular input $\mathbf{a}(t=0) = \frac{1}{2}(\sqrt{2}, -1, 0, 1)$, which is to be written to an input WP with a shaped write pulse at $t \sim -1.3$ ps. The population spectrum displayed in Fig. 2 (a) (i) shows that the population

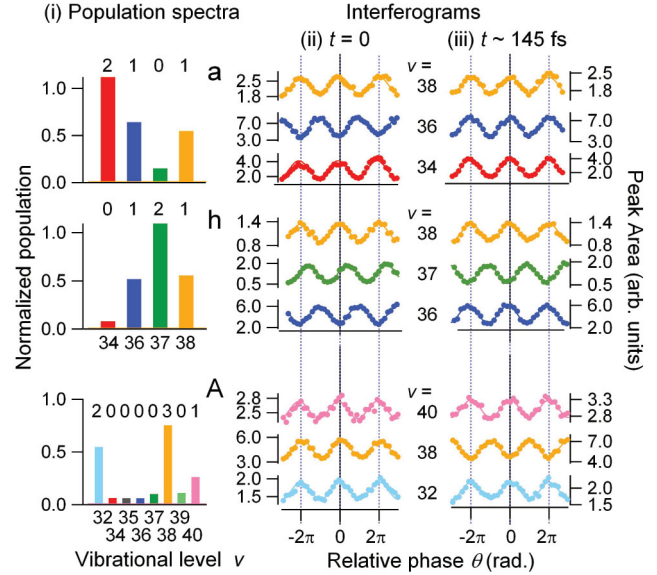


FIG. 2 (color). Input and output of the UFFT. (i) Population spectra; (ii) and (iii) interferograms of the input and reference WPs at $t = 0$ fs and ~ 145 fs. (a), (h), and (A) represent the results obtained with the inputs (a), (h), and (A) listed in Table I and the supplementary material [23]. The same color denotes the same vibrational level among (i), (ii), and (iii). The origin of the relative phase ($\theta = 0$) is arbitrary, and it denotes the position of the peak of the interferograms of $v = 38$ for (a) and (h), and $v = 32$ for (A). Dots are measured data, and solid lines are the sine functions least-square fitted to the measured interferograms with their periods fixed to 2π . The measurement of each interferogram and its least-square fitting have been carried out for a broader range of θ [25].

ratio is almost 2:1:0:1 ($= |\frac{\sqrt{2}}{2}|^2 : |-1|^2 : |0|^2 : |\frac{1}{2}|^2$). Measuring the absolute population is not essential since FT is a linear transform. The interferogram around $t = 0$ displayed in Fig. 2 (a) (ii) shows that the phase $\delta_{36}(t = 0)$ is shifted by $\sim \pi$ from $\delta_{34}(t = 0)$ and $\delta_{38}(t = 0)$. Therefore it is experimentally verified that the molecular input $\mathbf{a}(t = 0) = \frac{1}{2}(\sqrt{2}, -1, 0, 1)$ is almost realized in the input WP. It is seen, on the other hand, that the interferogram around $t \sim 145$ fs displayed in Fig. 2 (a) (iii) shows the phase $\delta_{36}(t \sim 145$ fs) is shifted by $\sim \pi$ from $\delta_{36}(t = 0)$ to be almost in phase with $\delta_{34}(t \sim 145$ fs) and $\delta_{38}(t \sim 145$ fs) in the molecular output. The population ratio is reasonably regarded to be constant for 145 fs since a typical life time of the B state is about $1 \mu\text{s}$ [26]. Therefore the correct molecular output $\mathbf{a}(t \sim 145$ fs) $= \frac{1}{2}(\sqrt{2}, 1, 0, 1)$ is almost realized to be back transformed by \mathbf{w}_4 to the output $\mathbf{f}^{\text{out}} = \frac{1}{2}(1, 1, 1, 1)$. Figure 2 (h) shows another example with the complex input $\mathbf{f}^{\text{in}} = \frac{1}{2}(1, -i, -1, i)$. The population spectrum and the interferograms displayed in Fig. 2 (h) show that the correct molecular input $\mathbf{a}(t = 0) = \frac{1}{2}(0, -1, \sqrt{2}, 1)$ and output $\mathbf{a}(t \sim 145$ fs) $= \frac{1}{2}(0, 1, -\sqrt{2}, 1)$ are almost realized to give the output $\mathbf{f}^{\text{out}} = (0, 1, 0, 0)$.

The performance of our UFFT has been quantitatively evaluated with a preparation fidelity and a transform accu-

racy [27]. The preparation fidelity is defined as $|\mathbf{a}^*(t=0) \cdot \mathbf{w}_4^{-1} \mathbf{f}^{\text{in}}|^2$, where $\mathbf{a}(t=0)$ and $\mathbf{w}_4^{-1} \mathbf{f}^{\text{in}}$ are the measured and expected coefficients at $t=0$, respectively, and $\mathbf{a}(t)$ is normalized as $|\mathbf{a}(t)|^2 = 1$ for arbitrary t . The transform accuracy is defined as $|\mathbf{a}^*(t \sim 145 \text{ fs}) \cdot \mathbf{w}_4^{-1} \mathbf{G}_4 \mathbf{w}_4 \mathbf{a}(t=0)|^2 = |\mathbf{a}^*(t \sim 145 \text{ fs}) \cdot \mathbf{D}_4 \mathbf{a}(t=0)|^2$, where $\mathbf{a}(t \sim 145 \text{ fs})$ and $\mathbf{w}_4^{-1} \mathbf{G}_4 \mathbf{w}_4 \mathbf{a}(t=0)$ are the measured and expected coefficients at $t \sim 145 \text{ fs}$ for measured $\mathbf{a}(t=0)$. These quantities have been evaluated for two sets of basis-function inputs listed in Table I to be better than 0.9, which are comparable to those obtained in the preceding ion-trap experiment [27]. The experimental uncertainties of our preparation fidelities and transform accuracies are also shown in Table I. The details of these uncertainties and their possible sources are given in the supplementary material [23].

We have also implemented eight-element UFFT with $v = 32$ and $34\text{--}40$ for $\mathbf{f}^{\text{in}} = \frac{1}{2}(0, 1, 0, 1, 0, 1, 0, 1)$ and $\mathbf{f}^{\text{out}} = \frac{1}{\sqrt{2}}(1, 0, 0, 0, -1, 0, 0, 0)$, and the corresponding molecular input $\frac{1}{\sqrt{6}}(\sqrt{2}, 0, 0, 0, 0, \sqrt{3}, 0, 1)$ and output $\frac{1}{\sqrt{6}}(\sqrt{2}, 0, 0, 0, 0, -\sqrt{3}, 0, 1)$, as shown in Fig. 2 (A). The relevant transform matrices are given in the supplementary material [23].

This ultrafast phase evolution can be applied to other logic gates. We have already proposed the controlled NOT (CNOT) gate [28] with the evolution time to be $\frac{1}{2}T_{\text{vib}}$ for the same sets of vibrational eigenstates [29]. In one of few pioneering experiments regarding implementation of a MEIP logic gate [19], Amitay and co-workers assigned the “yes” output of a classical AND gate to a specific temporal evolution of a WP, employing their local definition and one particular input available only within that experiment. In our present study, however, we have demonstrated a conceptually new MEIP logic gate, where we have utilized the temporal evolutions of a WP as gate operations according to their universal definitions with any arbitrary input.

Another promising approach to logic gates in MEIP has been proposed, based on population transfer with shaped intense laser pulses in the nonperturbative regime [13–18]. This includes four-element DFT with a 6-ps shaped pulse proposed theoretically [13]. Compared with this strong field approach, our free propagation approach may be less universal, but has better energy efficiency and fidelity. These two approaches could complement each other.

In the present demonstration of MEIP, read and write operations have been executed with an ensemble of jet-cooled molecules. Addressing of each molecule will be necessary for the future scalability. Rapid progress in the preparation of cold molecules in magnetic traps [30], in optical dipole traps [31], or in quantum solids [32] will hopefully be useful for this single-molecule addressing to be combined with our ultrafast MEIP approach.

The authors gratefully acknowledge Professor Akira Furusawa (The University of Tokyo), Professor Nobuyuki

Imoto (Osaka University), and Professor Nobuyuki Takei (IMS) for valuable discussion and their careful reading of this manuscript.

*ohmori@ims.ac.jp

- [1] International Technology Roadmap for Semiconductors, <http://www.itrs.net/>.
- [2] J. E. Green *et al.*, *Nature (London)* **445**, 414 (2007).
- [3] D. DeMille, *Phys. Rev. Lett.* **88**, 067901 (2002).
- [4] A. Micheli, G. K. Brennen, and P. Zoller, *Nature Phys.* **2**, 341 (2006).
- [5] A. Andre *et al.*, *Nature Phys.* **2**, 636 (2006).
- [6] K. Ohmori *et al.*, *Phys. Rev. Lett.* **96**, 093002 (2006).
- [7] H. Katsuki *et al.*, *Phys. Rev. A* **76**, 013403 (2007).
- [8] H. Katsuki *et al.*, *Phys. Rev. Lett.* **102**, 103602 (2009).
- [9] T. J. Dunn *et al.*, *Phys. Rev. Lett.* **70**, 3388 (1993).
- [10] T. C. Weinacht, J. Ahn, and P. H. Bucksbaum, *Phys. Rev. Lett.* **80**, 5508 (1998).
- [11] H. Katsuki *et al.*, *Science* **311**, 1589 (2006).
- [12] A. Monmayrant, B. Chatel, and B. Girard, *Phys. Rev. Lett.* **96**, 103002 (2006).
- [13] J. P. Palao and R. Kosloff, *Phys. Rev. Lett.* **89**, 188301 (2002).
- [14] J. P. Palao and R. Kosloff, *Phys. Rev. A* **68**, 062308 (2003).
- [15] C. M. Tesch and R. de Vivie-Riedle, *Phys. Rev. Lett.* **89**, 157901 (2002).
- [16] R. de Vivie-Riedle and U. Troppmann, *Chem. Rev.* **107**, 5082 (2007).
- [17] C. Gollub, M. Kowalewski, and R. de Vivie-Riedle, *Phys. Rev. Lett.* **101**, 073002 (2008).
- [18] Y. Ohtsuki, *Chem. Phys. Lett.* **404**, 126 (2005).
- [19] Z. Amitay, R. Kosloff, and S. R. Leone, *Chem. Phys. Lett.* **359**, 8 (2002).
- [20] J. Vala *et al.*, *Phys. Rev. A* **66**, 062316 (2002).
- [21] R. N. Bracewell, *The Fourier Transform and Its Applications* (McGraw-Hill, New York, 1978).
- [22] P. W. Shor, in *Proceedings of the 35th Annual Symposium on Foundations of Computer Science*, edited by S. Goldwasser (IEEE Computer Society Press, Los Alamitos, CA, 1994), p. 124.
- [23] See supplementary material at <http://link.aps.org/supplemental/10.1103/PhysRevLett.104.180501> for the details of the transform matrices, inputs and outputs, interferometer, and uncertainties.
- [24] The maximum clock rate of IBM Power 6 is 5.0 GHz, giving its clock period to be 200 ps.
- [25] K. Hosaka *et al.* (to be published).
- [26] J. A. Paisner and R. Wallenstein, *J. Chem. Phys.* **61**, 4317 (1974).
- [27] J. Chiaverini *et al.*, *Science* **308**, 997 (2005).
- [28] M. A. Nielsen and I. L. Chuang, *Quantum Computation and Quantum Information* (Cambridge University Press, Cambridge, 2000).
- [29] Y. Teranishi *et al.*, *J. Chem. Phys.* **124**, 114110 (2006).
- [30] J. D. Weinstein *et al.*, *Nature (London)* **395**, 148 (1998).
- [31] K.-K. Ni *et al.*, *Science* **322**, 231 (2008).
- [32] H. Katsuki and T. Momose, *Phys. Rev. Lett.* **84**, 3286 (2000).